International Journal of Applied Earth Observation and Geoinformation 136 (2025) 104380

Contents lists available at ScienceDirect

International Journal of Applied Earth Observation and Geoinformation

journal homepage: www.elsevier.com/locate/jag

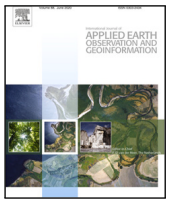

Empirical methods to determine surface air temperature from satellite-retrieved data

Joan Vedrí [a,*], Raquel Niclòs [a], Lluís Pérez-Planells [b], Enric Valor [a], Yolanda Luna [c], María José Estrela [d]

[a] Department of Earth Physics and Thermodynamics, Faculty of Physics, University of Valencia, Dr. Moliner 50, Burjassot, 46100, Valencia, Spain
[b] IMK - ASF, Karlsruhe Institute of Technology (KIT), Hermann-von-Helmholtz-Platz 1, Karlsruhe, 76344, Eggenstein-Leopoldshafen, Germany
[c] Agencia Estatal de Meteorología (AEMET), Spain
[d] Department of Geography, Faculty of Geography and History, University of Valencia, Blasco Ibañez 28, Valencia, 46010, Spain

ARTICLE INFO

Keywords:
Surface air temperature
Land surface temperature
Climate change
Essential climate variable
Machine learning

ABSTRACT

Surface air temperature (SAT) is an essential climate variable (ECV). Models based on remote sensing data allow us to study SAT, without the need for a large network of meteorological stations. Therefore, it allows monitoring the climate in remote and extensive areas. Niclos et al. (2014) proposed parametric equations for the SAT retrieval over the Spanish Mediterranean basins. In this study, we evaluated those equations, but in a larger area and period of study. In addition, we proposed several linear regression models and nonlinear models based on decision tree methods, non-parametric methods and neuronal networks. These models relate SAT to land surface temperature, vegetation indexes and albedo from MODIS data. Moreover, meteorological reanalysis data, from ERA5-Land database, and geographical parameters were used. The accuracy of each model was evaluated against data from meteorological stations operated by AEMET in the Spanish Mediterranean basins, during the period 2021–2022. The equations of Niclos et al. (2014) obtained a robust root mean square error (RRMSE) of 3.1 K at daytime and 1.9 K at nighttime. For the linear regression models, the RRMSE decreased to 2.3 K (1.5 K) at daytime (nighttime). Finally, the nonlinear methods, in particular XGBoost model, showed an RRMSE of 1.5 K for daytime and 1.0 K at nighttime. Therefore, the comparison between methods showed that nonlinear models, in particular those based on decision tree methods, offered the best results in SAT retrieval in our study.

1. Introduction

GCOS defined the surface air temperature (SAT) as an ECV. It has an important role on evaluating climate change (GCOS, 2022), affecting many aspects of humans life, e.g. public health or agricultural sector (Paredes-Fortuny and Khodayar, 2023; Zakšek and Schroedter-Homscheidt, 2009).

Currently, huge nets of meteorological stations installed around the world provide ground mesurements of meteorological variables, e.g. SAT (Brugnara et al., 2019; Dunn et al., 2020). Even so, the stations layout presents gaps located in remote zones due to extreme weather conditions or economic reasons (Dunn, 2020). Remote sensing data allow us to estimate SAT over a large region without the need for a dense network of meteorological stations (Czajkowski et al., 2000).

Previous studies suggested that land surface temperature (LST) has a high correlation with SAT, estimating it from LST and Spectral Vegetation Index measurements (SVI) (Khesali and Mobasheri, 2023; Nieto et al., 2011; Prihodko and Goward, 1997). Other studies found that, although SAT is mainly related to LST, it is also related to geographical and meteorological parameters (Cristóbal et al., 2008; Ninyerola et al., 2007). Thus, adding more parameters results in an improvement on the SAT retrieval (Cristóbal et al., 2008; Niclos et al., 2014).

Linear methods have been typically used for the estimation of SAT, with accuracies between 1.2 and 4 °C depending on input parameters, study region and period (Cristóbal et al., 2008; Khesali and Mobasheri, 2020; Niclos et al., 2014; Nieto et al., 2011; Parlak and Yavasoglu, 2023; Prihodko and Goward, 1997). In the last decade, nonlinear models based on machine learning and deep learning have been applied as an alternative to linear methods for SAT retrieval, achieving also more accurate results (Noi et al., 2017; Parlak and Yavasoglu, 2023; Ruiz-Álvarez et al., 2019; Ye et al., 2022). Noi et al. (2017) and Parlak and Yavasoglu (2023) compared the linear and nonlinear methods using a reduced number of variables. The comparison yielded to similar

* Corresponding author.
E-mail address: joan.vedri@uv.es (J. Vedrí).

https://doi.org/10.1016/j.jag.2025.104380
Received 2 October 2024; Received in revised form 16 December 2024; Accepted 14 January 2025
Available online 23 January 2025

results between both methods.

In this paper we retrieve the SAT with linear and nonlinear methods using a larger number of variables, which includes satellite data, meteorological data, geographical and topographical parameters. Previous studies obtained good accuracies for small areas (<25000 km^2) but they tend to worse accuracies when their areas are larger. In addition, nonlinear techniques are applied for first time over the Spanish Mediterranean Basins which cover a relevant climatological area (~150000 km^2) due to its location and orography (Bladé and Castro-Díez, 2010; Font Tullot, 2000; Gonzalez-Hidalgo et al., 2015; Pompeu et al., 2023), and it has been identified as a hotspot in Europe in terms of climate (Diffenbaugh and Giorgi, 2012; Stocker et al., 2023), making this study also important in terms of climate change monitoring.

Moderate Resolution Imaging Spectroradiometer (MODIS), aboard Terra and Aqua platforms, acquires daily data in 36 spectral bands. MODIS data were used previously to retrieve the SAT due to its temporal and spatial resolution (Khesali and Mobasheri, 2023; Niclos et al., 2014; Noi et al., 2017; Recondo et al., 2013). In particular, we used Aqua MODIS which offers us 2 daily data for LST, giving us the possibility to obtain and compare daytime and nighttime models. In Niclos et al. (2014) the authors used MODIS data and ground data to retieve SAT along Valencian region during 2009 summer. In this study we extended the area and period of their study, covering all Spanish Mediterranean region during 2 years (2021–2022). Thus, we first studied the possibility of extrapolating the regressions obtained by Niclos et al. (2014) for the entire Spanish Mediterranean region.

Thus, our main goal is to retrieve the SAT from multiple variables, e.g. satellite data, meteorological data, geographical and topographical parameters, for the Spanish Mediterranean basins, using linear and nonlinear methods. Furthermore, we aimed to obtain an accurate and generalized model over the area of study, which is representative of different climates, landcovers and elevation range, with an accuracy similar or better than that found in the existing literature for smaller areas.

In the following section the study area and the data are defined. Then, the metodology followed in this study is explained in Section 3. The results obtained are shown and discussed in Section 4 and, finally, the main conclusions of this study are summarized in Section 5.

2. Study area and data

2.1. Study area

Spanish Mediterranean basins are located on the east side of the Iberian Peninsula, but include also the Balearic Islands (Fig. 1). Our study area presents a wide variety of land covers and terrain elevation range. The predominant climate on Spanish Mediterranean basins is hot-summer Mediterranean climate, which has dry summers and wet winters with a moderate temperature variation between seasons (AEMET, 2011).

In addition, Mediterranean region is suffering an increase in its temperature, which is higher compared to other regions around the world (Lionello and Scarascia, 2018; MedECC, 2020). Also, the severity and periodicity of extreme climate events, e.g. tropical nights, torrential rainfalls or heat waves, are increasing over the Spanish Mediterranean basins during the last 7 decades analyzed (Lorenzo et al., 2021; Lorenzo and Alvarez, 2022; Miró et al., 2018; Olcina et al., 2019; Paredes-Fortuny and Khodayar, 2023), making the region a relevant study area for analyzing climate change.

2.2. In situ and meteorological data

Fig. 1 shows the distribution of the ground measurements employed in this study. These stations are distributed along 8 river basins that flow into the Mediterranean Sea. We used SAT values from them to validate models results. The other variables were obtained from ERA5-Land reanalysis database, which provides hourly data for different meteorological variables with a native resolution of 9 km (Muñoz-Sabater et al., 2021). ERA5-Land was proved to be a good database to reproduce spatio-temporal trends over Spain (Gomis-Cebolla et al., 2023).

Relative humidity (RH), wind velocity (U) and solar irradiance (I) cannot be directly extracted from ERA5-Land. To obtain relative humidity we used a version of the August-Roche-Magnus equation (August, 1828; Magnus, 1844):

$$RH = \frac{e^{\frac{\beta \cdot T_d}{\lambda + T_d}}}{e^{\frac{\beta \cdot T_a}{\lambda + T_a}}} \cdot 100 \quad (1)$$

where $\beta = 17.625$ and $\lambda = 243.04$ °C are the recommended values for Magnus' coefficients (Alduchov and Eskridge, 1996; Lawrence, 2005). T_d and T_a represent dew point temperature and SAT, respectively, which can be downloaded directly from ERA5-Land.

Wind speed was obtained by calculating the modulus of the vertical and horizontal components of the wind provided in the ERA5-Land database. Finally, solar irradiance was obtained from the downwards surface solar radiation, which was converted into solar irradiance by the difference of the accumulated radiation between each hour divided by 3600 s.

2.3. Remote sensing data

Remote Sensing data were used to obtain LST, normalized difference vegetation index (NDVI) and albedo (AL) variables. LST was obtained from the MYD11A1 MODIS product, which have daily temporal resolution and 1 km nominal spatial resolution (Wan, 1999). MYD11A1 product gives two LST values per day, one at daytime and the other at nighttime. Daytime data are measured between 12:00 and 14:00 UTC at the study area, while nighttime data are measured between 1:00 and 3:00 UTC. Thus, since Aqua overpasses are closer to maximum and minimum daily temperatures, its observations are more suitable for climate studies (Good, 2015, 2016; Good et al., 2017) than those from MODIS Terra, which has an overpass time around 10 AM/PM, i.e. short after mid-night and after sunrise respectively. LST data were filtered to remove all values that were obtained with a view angle greater than 45°, to avoid overlapping pixels between two orbits, and those with an error greater than 2 K. Filtering large viewing angles also reduces the directional effects introduced in the edges of the images with large swaths due to the directional anisotropy in the observations. Both LST and NDVI were demonstrated to be sensible to these effects, so this filtering improved the accuracy of our data (Bian et al., 2023; León-Tavares et al., 2021). NDVI data were extracted from the MYD13A2 MODIS product, which has 16-day temporal resolution and 1 km spatial resolution (Huete and Justice, 1999). Due to NDVI's stability, NDVI values were processed to obtain daily values, by searching the nearest value measured for each day. Finally, albedo data were extracted from the MCD43A3 MODIS product, which has daily temporal resolution and 500 m spatial resolution (Strahler and Muller, 1999). Albedo values were resampled to 1 km by calculating the mean value of 2 × 2 pixels, in order to homogenize all product spatial resolutions.

2.4. Geographical and topographical data

Geographical and topographical data influence SAT (Cristóbal et al., 2008; Niclos et al., 2014; Ninyerola et al., 2007; Zakšek and Schroedter-Homscheidt, 2009). In particular, the following geographical and topographical parameters were used: elevation (h), longitude (Lon), latitude (Lat), topographical aspect (ϕ_t), slope (s) and the difference between each station altitude and the mean elevation of its 20 km around it (Δh).

These parameters were computed using a 1 km resolution resampled digital elevation model (DEM) mosaic made from sheets of the Spanish

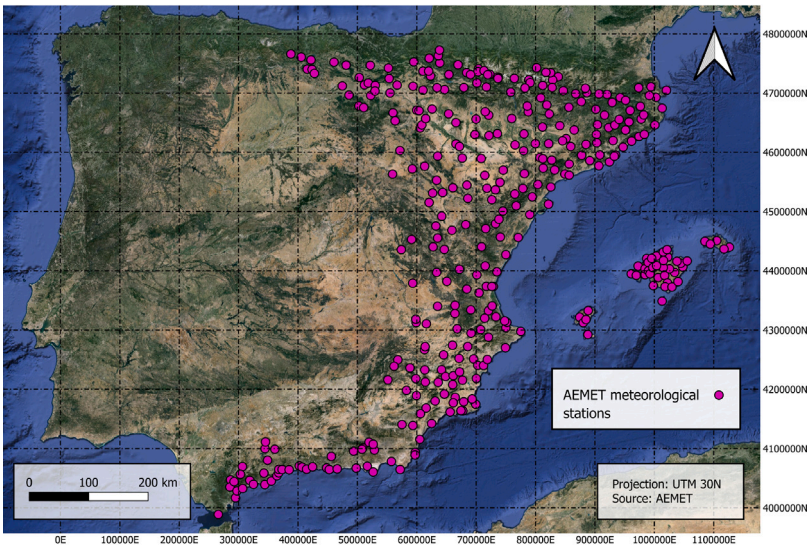

Fig. 1. Location of AEMET meteorological stations in the Spanish Mediterranean basins.

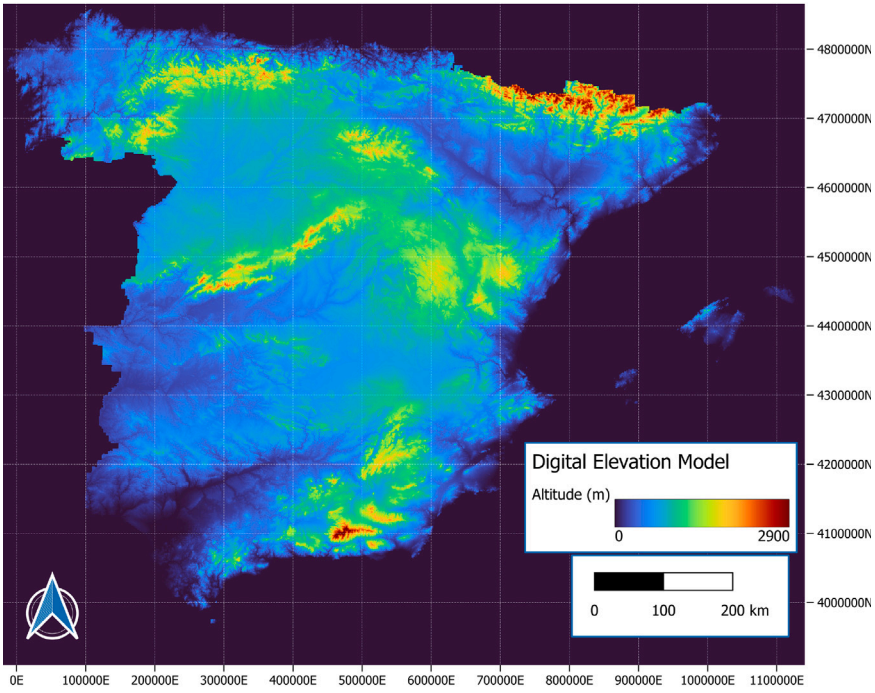

Fig. 2. Study area's DEM.

National Geography Institute (IGN; IGN, 2010) in UTM 30 projection (Fig. 2), and the coastline database from the European Environment Agency (EEA; EEA, 2017).

In addition, solar coordinates were used, such as solar zenithal angle (z), solar azimuthal angle (a) and solar incidence angle (i) calculated with the expressions published in Valor et al. (2023). These variables characterize how solar radiation affects the study area, taking into account its orography and the day and hour of the satellite overpass. Solar coordinates, together with remote sensing data and meteorological data which offer instantaneous data, are thus time-dependent variables.

All these variables were obtained for the period 2021–2022, but, not everyday were available due to some factors, e.g. the presence of clouds, low LST accuracy and lack of in situ data. Thus, we filtered all the variable out from those days with missing values. Finally, the database was splitted into two datasets, one with daytime values and another with nighttime values. Table 1 shows the statistics (mean (M), standard deviation (SD), maximum (Max) and minimum (Min)) for the studied variables in the final datasets.

Once we got the daytime and nighttime datasets, we filtered the data to eliminate values located in the 2% of the tails of the SAT histograms to avoid outliers. This process removed all extreme values

Table 1
Inputs' statistics for daytime and nighttime.

	Daytime inputs				Nighttime inputs			
	M	SD	Min	Max	M	SD	Min	Max
LST (K)	302	12	265	329	282	7	255	301
NDVI	0.4	0.15	−0.11	0.9	0.4	0.15	−0.11	0.9
Al	0.16	0.05	0.03	0.7	0.17	0.04	0.03	0.7
SAT (K)	296	8	269	317	284	8	257	310
RH (%)	45	14	9	99	83	14	17	100
U (m/s)	3	1.7	0.03	16	2.1	1.4	0.02	15
I (10^3 W/m^2)	0.7	0.2	0.1	1.0				
Lat (°)	40	2	35	43	40	2	36	43
Lon (°)	−0.4	2.3	−5	4	−0.5	2.2	−5	4
h (km)	0.5	0.4	0	2.3	0.5	0.4	0	2.3
Δh (km)	−0.08	0.18	−0.9	0.7	−0.08	0.18	−0.9	0.7
s (°)	3	3	0	19	3	3	0	19
ϕ_t (°)	160	99	1	359	162	98	1	359
dist (km)	27	25	0	91	27	26	0	91
z (rad)	0.7	0.3	0.2	1.2				
a (rad)	−0.5	0.2	−1.2	0.0				
i (rad)	0.7	0.3	0.1	1.4				

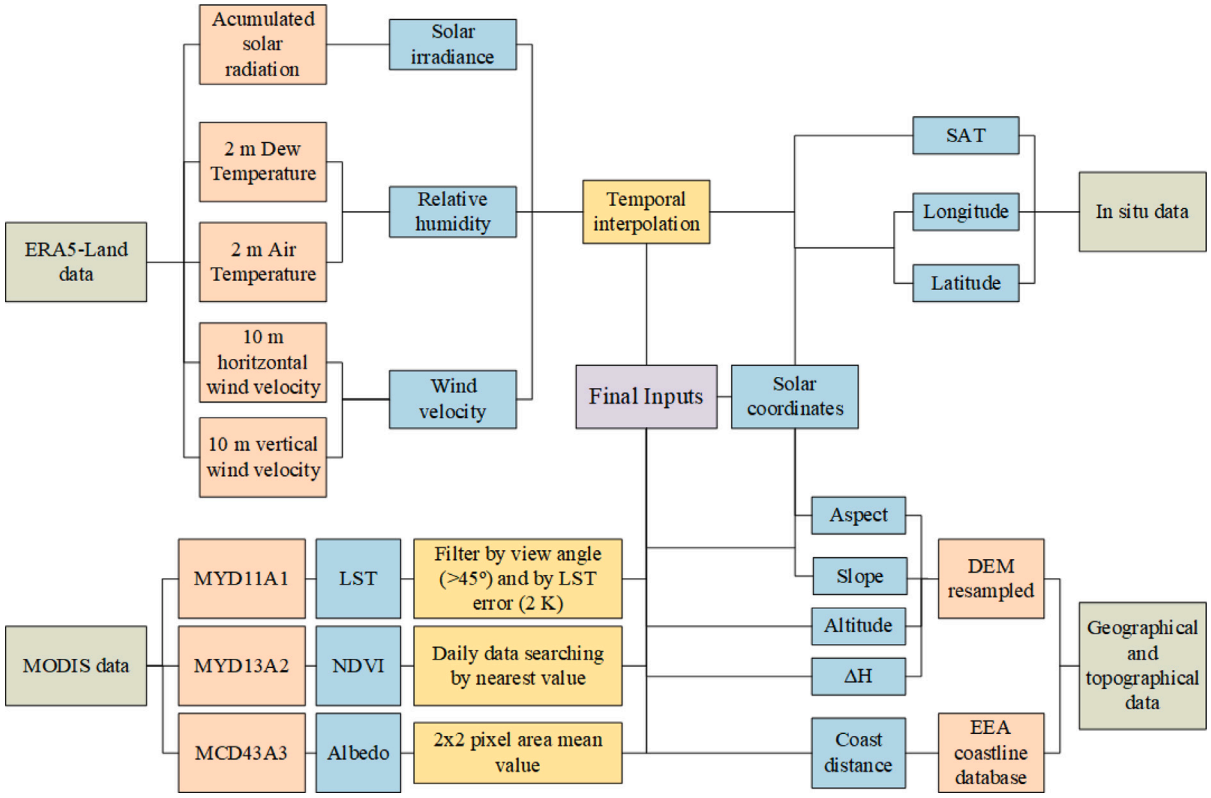

Fig. 3. Flowchart of data processing.

that could interact with the robustness of our models (Ghent et al., 2019).

The procedure detailed in this section is summarized in Fig. 3.

3. Methods

This section describes the different models analyzed in the study. We divided them in 3 groups: regressions published in Niclos et al. (2014), linear methods and nonlinear methods.

Firstly, we described the regressions published in Niclos et al. (2014), which were evaluated in our extended study region .

Among linear regression models, we have regularized and non-regularized methods. Most of the previous studies Cristóbal et al. (2008), Niclos et al. (2014), Nieto et al. (2011), Noi et al. (2017), Parlak and Yavasoglu (2023), Prihodko and Goward (1997), Ruiz-Álvarez et al. (2019) and Ye et al. (2022) used non-regularized methods, achieving good results. Parlak and Yavasoglu (2023) also studied regularized methods showing a good improvement over non-regularized. We used

Table 2
Regressions published in Niclos et al. (2014) for daytime and nighttime.

	Daytime equations
D.1	$SAT = 0.40\ LST + 178.7$
D.2	$SAT = 0.26\ LST - 12.4\ (1 - NDVI) - 5.9\ I - 0.102\ RH - 0.031\ Lat - 0.8\ h + 27.0\ AL + 260.1$
D.3	$SAT = 0.25\ LST - 9.3\ (1 - NDVI) - 8.8\ (1 - AL)\ I - 0.109\ RH - 0.029\ Lat - 2.2\ h - 0.57\ Dist + 264.6$
D.4	$SAT = 0.47\ LST - 18.6\ (1 - NDVI) - 6.0\ I - 0.040\ Lat + 1.9\ h - 0.101\ Dist + 44.4\ AL + 195.6$
D.5	$SAT = 0.49\ LST - 13.5\ (1 - NDVI) - 10.5\ (1 - AL)\ I - 0.037\ Lat - 0.5\ h - 0.056\ Dist + 194.6$
D.6	$SAT = LST + 1.82 - 10.66 \cos z\ (1 - NDVI) - 0.566\ a - 3.72\ (1 - AL)(\cos I / \cos z + (\pi - s)/\pi)\ I - 3.41\ \Delta h$
D.7	$SAT = 0.52LST + 152.7 - 8.6 \cos z\ (1 - NDVI) + 1.4\ a - 4.1\ (1 - AL)(\cos I / \cos z + (\pi - s)/\pi)\ I - 2.9\ \Delta h$
D.8	$SAT = 0.52LST + 152.3 - 8.5 \cos z\ (1 - NDVI) - 5.4\ (1 - AL)(\cos I / \cos z + (\pi - s)/\pi)\ I$
D.9	$SAT = 0.23LST - 9.5 \cos z\ (1 - NDVI) - 2.3\ (1 - AL)(\cos I / \cos z + (\pi - s)/\pi)\ I - 0.115\ RH - 0.033\ Lat - 2.8\ h - 0.059\ Dist + 270.4$
D.10	$SAT = 0.51LST - 15.1 \cos z\ (1 - NDVI) - 3.1\ (1 - AL)(\cos I / \cos z + (\pi - s)/\pi)\ I - 0.04\ Lat - 1.0\ h - 0.059\ Dist + 188.5$
	Nighttime equations
N.1	$SAT = 0.94LST + 19.3$
N.2	$SAT = 0.85LST + 1.8(1 - NDVI) - 0.129\ RH + 0.0005\ RH^2 - 0.009\ Lat - 0.8\ h - 0.009\ Dist - 10.4\ AL + 0.04\ U + 58.9$
N.3	$SAT = 0.86LST + 1.7(1 - NDVI) - 0.130\ RH + 0.0005\ RH^2 - 0.009\ Lat - 0.7\ h - 0.008\ Dist - 10.6\ AL + 56.1$
N.4	$SAT = 0.92LST + 2.8(1 - NDVI) - 0.012\ Lat - 0.9\ h - 0.0018\ Dist - 11.4\ AL + 0.26\ U + 31.8$
N.5	$SAT = 0.99LST + 2.3(1 - NDVI) - 0.012\ Lat - 1.3\ h - 0.0016\ Dist - 13.3\ AL + 12.2$

Ordinary Least Squares (OLS) as non-regularized method, while Ridge, Lasso and Elastic Net (EN) were chosen as regularized methods.

In the last decade, nonlinear methods have been used frequently. Random Forest (RF) is one of the most popular nonlinear method to obtain SAT (Noi et al., 2017; Parlak and Yavasoglu, 2023; Ruiz-Álvarez et al., 2019), although several authors applied other approaches e.g. neuronal networks (Ye et al., 2022). In our study we also used different approaches to test which one offers the best results. These models are RF, XGBoost (XGB), K-Nearest Neighbors (KNN) and a Multilayer Perceptron (MLP) neuronal network.

To validate our results and prevent overfitting, we used a holdout of 70%/30% for training and test, respectively. In addition, each method had a 10-fold cross validation to made our results more robust to overfitting (James et al., 2013; Montavon et al., 2012). We used the Scikit-learn Python's library (Pedregosa et al., 2011a,b).

3.1. Niclos et al. (2014) regressions

Niclos et al. (2014) included 15 equations, 10 for daytime and 5 for nighttime (Table 2). They studied the retrieval of the SAT during 2009 summer over the Valencian region. One of these equations (D.6 in Niclos et al., 2014) was proposed by Zakšek and Schroedter-Homscheidt (2009), while the others were proposed by Niclos et al. (2014) using stepwise algorithms. We evaluated their expressions using our dataset, which covers a larger region and a longer period.

3.2. Linear methods

Many authors pointed out that SAT has a linear dependence with LST and other parameters (Cristóbal et al., 2008; Niclos et al., 2014; Nieto et al., 2011; Prihodko and Goward, 1997). We studied linear dependence among SAT and the selected input variables shown in Table 1. Using linear methods require that the used variables must accomplish certain major assumptions, which are: weak exogeneity, linearity, homoscedasticity, independence of errors, lack of perfect multicollinearity and assumption of zero mean of residuals (Hayashi, 2000), which in this study are estimated as the difference between the predicted and observed SAT (Jeng and Martin, 1985). The correlation matrixes for daytime and nighttime using Pearson's method showed that LST has the highest linear dependence with SAT (Fig. 4). Since some variables have linear relation with the difference between SAT and LST, but not with SAT only, those variables with a linear dependence higher than 10% or a linear dependence with the difference between SAT and LST higher than 10% were considered for the regressions. Applying these

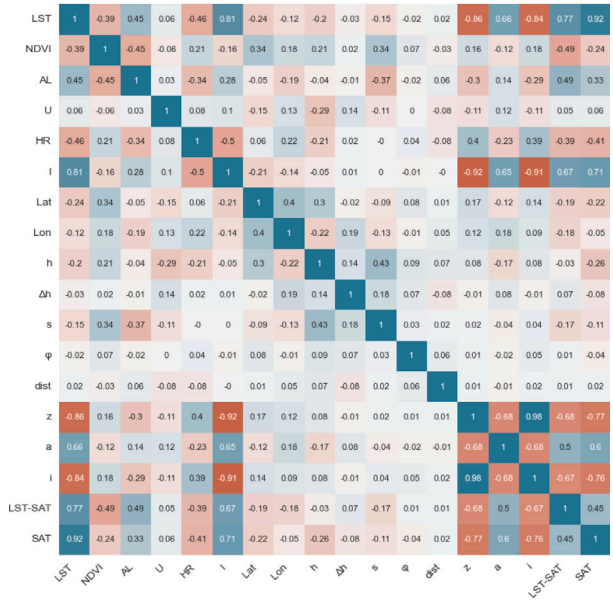

Fig. 4. Correlation matrix for daytime values.

requirements, wind velocity (U), distance to coast (dist), the difference between each station altitude and the mean elevation of its 20 km around it (Δh), and aspect (ϕ_t) were dropped out for daytime linear models. For nighttime models, slope (s), aspect (ϕ_t) and distance to coast (dist) were dropped out. Homoscedasticity was studied by the analysis of residuals (Fig. 5). Independence of errors and lack of perfect multicollinearity were accomplished due to the feature selection of the regularized methods (Tibshirani, 2011; Williams et al., 2013).

Regularized regressions are useful to prevent overfitting by reducing the dimensionality of data, specially when the amount of samples is lower than the amount of parameters (Schelldorfer et al., 2011), which is not our case but helps also to avoid multicollinearity issues.

Finding the best parameters for our regressions is crucial to obtain the best fit of the linear model. In order to achieve it, we looked for the best α value for each regularized regressions and the best ρ value for the EN. As it is shown in Fig. 6 and Table 3, α values are close to 0 on all methods, meaning that their results are going to be similar to

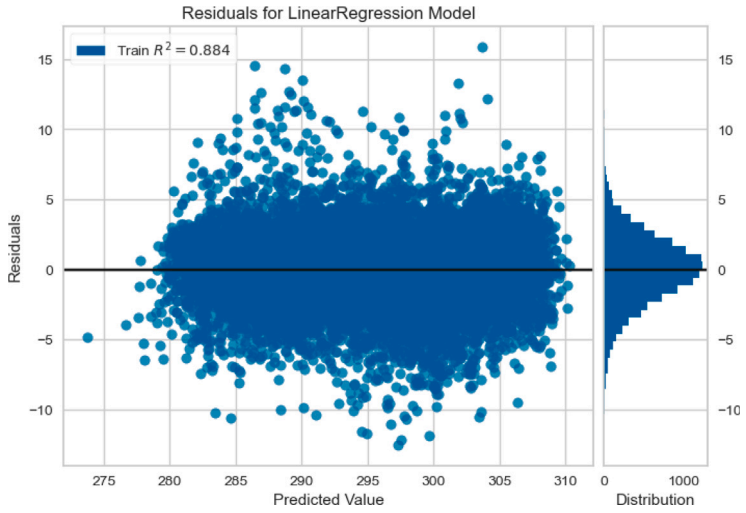

Fig. 5. Residuals analysis, gaussian distribution shows homoscedasticity.

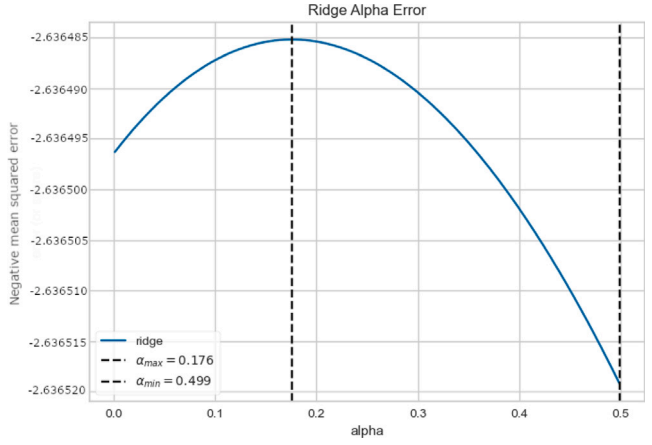

Fig. 6. Best α finding example for Ridge method at daytime.

Table 3
α values for each linear method.

α	Ridge	Lasso	EN
Daytime	0.176	<0.001	<0.001
Nighttime	0.654	<0.001	<0.001

Table 4
Optimized parameters for RF, XGB and KNN methods.

	RF		XGB		KNN	
	Daytime	Nighttime	Daytime	Nighttime	Daytime	Nighttime
Max depth	33	30	6	5	–	–
Number of estimators	502	483	1684	1425	–	–
Learning rate	–	–	0.052	0.025	–	–
K	–	–	–	–	5	2

Table 5
MLP's structure (number of neurons) and parameters for dense layers.

Number of neurons	Daytime	Nighttime
18	306	-
12	–	156
8	152	104
4	36	36
1	5	5

the OLS method (Hoerl and Kennard, 1970; Pedregosa et al., 2011a,b; Tibshirani, 1996; Zou and Hastie, 2005). For EN, $\rho = 0.98$ for daytime and 0.71 for nighttime.

3.3. Nonlinear methods

Since not all input variables showed a good linear correlation with SAT, that suggested that nonlinear methods can be a good approach for SAT retrieval. We studied 3 different approaches: (i) algorithms based on decision trees, i.e. RF and XGB, (ii) non-parametrical algorithms, i.e. KNN, (iii) and a neuronal network, i.e. MLP.

While RF was previously tested showing slightly better accuracies than linear methods (Noi et al., 2017; Parlak and Yavasoglu, 2023; Ruiz-Álvarez et al., 2019), XGB is an extreme gradient boosting algorithm which typically outperforms RF (Hastie et al., 2009; Shao et al., 2024; Zhang et al., 2022). KNN is a non-parametric model that computes the mean value of the k-nearest values for each point, fitting predictors' behavior to the reference value (Cover and Hart, 1967; Fix and Hodges, 1989).

All the previous methods requires a parametrization to be optimized. Parameters were extracted by using a random grid search providing an interval for each parameter and randomly choosing a combination of them, getting the best combination possible. Best parameters found are shown in Table 4.

MLP is a feedforward neuronal network which consists in multiple layers of neurons fully connected with each others. These kind of neuronal networks are the base of many others, e.g. convolutional neuronal networks and recurrent neuronal networks (Hastie et al., 2009). We used a simple network, due to the amount of available data in our study, with the structure that is shown on Table 5.

To compute all these methods we used different Python's libraries. For RF and KNN we used Scikit-learn library (Pedregosa et al., 2011a,b), for XGB we used XGBoost library (Chen and Guestrin, 2016) and Tensorflow for MLP method (Abadi et al., 2015).

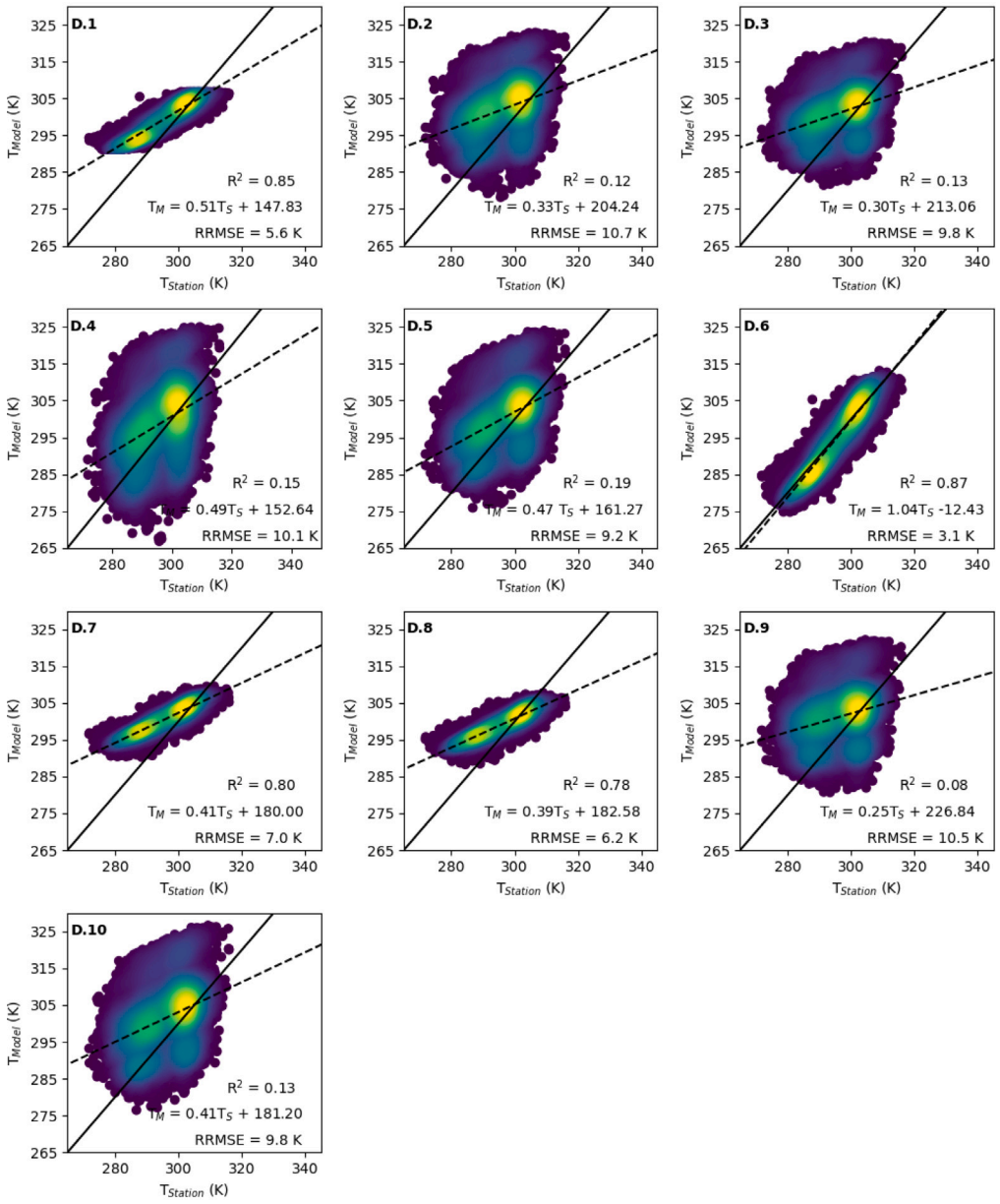

Fig. 7. SAT computed using the regressions published in Niclos et al. (2014) for daytime against in situ SAT.

3.4. Statistical comparison

To compare all the methods and analyze which performs the best, we used robust statistics (i.e., median (Med), robust standard deviation (RSD; Eq. (2)) (Wilrich, 2007; Pérez-Planells et al., 2021) and robust root-mean-square-error (RRMSE; Eq. (3))) to avoid the influence of possible outliers. Furthermore, we calculated also standard statistics (i.e., bias (B), standard deviation (SD), root-mean-square-error (RMSE)) for comparison with previous studies.

$$RSD = median\left|(T_{Model} - T_{Station})_i - median(T_{Model} - T_{Station})_i\right| \cdot 1.483 \quad (2)$$

$$RRMSE = \sqrt{Med^2 + RSD^2} \quad (3)$$

4. Results and discussion

This section includes the main results obtained. For all figures included hereafter the solid line represents the 1:1 relationship, while dashed line represents the linear fit between reference SAT and modeled SAT. Results are shown following the structure used on Section 3.

4.1. Niclos et al. (2014) regressions

Niclos et al. (2014) regressions applied to our dataset show an irregular behavior for daytime, where some regressions achieve high R^2 (e.g. D.6) while others gets low R^2 (e.g. D.9) (Fig. 7). The main difference between those that achieve high R^2 and those that not, is the coefficient given to the LST parameter. Those whose LST coefficient is closer to 1 have higher R^2, meaning that LST is the most important factor to retrieve SAT.

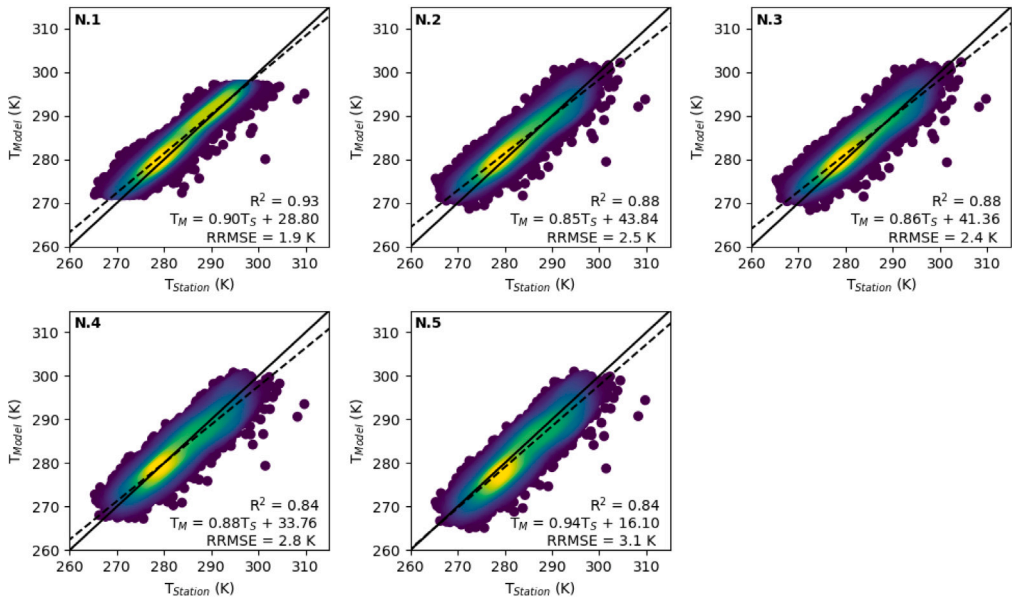

Fig. 8. SAT computed using the regressions published in Niclos et al. (2014) for nighttime against in situ SAT.

Table 6
Niclos et al. (2014) daytime regressions statistics of the differece between in situ SAT and computed SAT for our dataset.

	D.1 (K)	D.2 (K)	D.3 (K)	D.4 (K)	D.5 (K)	D.6 (K)	D.7 (K)	D.8 (K)	D.9 (K)	D.10 (K)
B	3.8	6.3	5.3	3.0	4.3	−0.6	4.9	3.4	5.4	5.4
SD	4.1	8.6	8.1	9.8	8.5	3.1	4.8	4.9	8.9	8.1
RMSE	5.6	10.6	9.7	10.2	9.5	3.2	6.9	6.0	10.4	9.8
Med	3.6	6.4	5.2	3.2	4.1	−0.7	4.5	2.9	5.3	5.3
RSD	4.2	8.5	8.2	9.5	8.2	3.1	5.4	5.5	9.1	8.2
RRMSE	5.6	10.7	9.8	10.1	9.2	3.1	7.0	6.2	10.5	9.8

Table 7
Niclos et al. (2014) nighttime regressions statistics of the differece between in situ SAT and computed SAT for our dataset.

	N.1 (K)	N.2 (K)	N.3 (K)	N.4 (K)	N.5 (K)
B	1.0	0.8	0.7	−0.4	−1.2
SD	1.9	2.4	2.4	2.8	2.9
RMSE	2.1	2.6	2.5	2.8	3.1
Med	1.0	0.9	0.7	−0.4	−1.2
RSD	1.6	2.3	2.3	2.7	2.8
RRMSE	1.9	2.5	2.4	2.8	3.1

For nighttime, the variation between expressions is lower (Fig. 8), being N.1 the best with $R^2 = 0.93$. In general nighttime results are better than daytime, as it was also found by other authors Niclos et al. (2014), Ruiz-Álvarez et al. (2019) and Tao et al. (2014). This behavior is related to the inputs used, because there are less variables involved in the SAT retrieval at nighttime, and LST gains importance against other variables.

These results also can be seen in the statistical results shown in Tables 6 and 7, where the lowest RMSE for daytime is for equation D.6, with 3.2 K, and the lowest nighttime RMSE is for equation N.1, with 2.1 K. These results do not resemble those obtained by Niclos et al. (2014). They found that, for daytime, D.6 was the worst expression with an RMSE of 3.37 K, while the best result was for D.2, with a RMSE of 1.28 K. For nighttime the results obtained by Niclos et al. (2014) showed that N.1 (the linear one with just LST) performed the worst, with an RMSE of 1.81 K while N.2 achieved the best result with 1.26 K.

RMSE for D.6 is similar in both studies meaning that Zakšek and Schroedter-Homscheidt (2009) expression works similar for different areas and periods, while Niclos et al. (2014) expressions depend more on the dataset used. This fact prevents Niclos et al. (2014) expressions from being extrapolated to longer areas and periods, although the coefficients of each equation can be reffited for other datasets.

4.2. Linear methods

Figs. 9 and 10 show scatterplots of station and computed SATs for daytime and nighttime linear methods.

As we advanced in Section 3.2, achieving low values for α's value indicates that there is no need to reduce the dimensionality of our dataset. In other words, all algorithms are being reduced to an OLS (Figs. 9 and 10). This means that our number of samples is enough to handle correlated errors without needing regularized methods.

Tables 8 and 9 show the RRMSE obtained by linear methods. RRMSE values are of 2.3 K for daytime and of 1.5 K for nighttime, which are much lower than those we obtained with Niclos et al. (2014) regressions (Tables 6 and 7). In fact, these methods outperformed the best regressions that we found before (D.6 and N.1).

We finally obtained, from the OLS method, the following expressions for retrieve SAT for daytime (Eq. (4)) and nighttime (Eq. (5)), respectively:

$$SAT = 0.807\ LST + 8.4\ NDVI - 13.6\ AL - 0.030\ HR - 5.9\ I - \\ - 0.063\ Lat + 0.073\ Lon - 1.98\ h + 0.080\ s + 1.8\ z + \\ + 1.1\ a - 1.3\ i + 59.9 \quad (4)$$

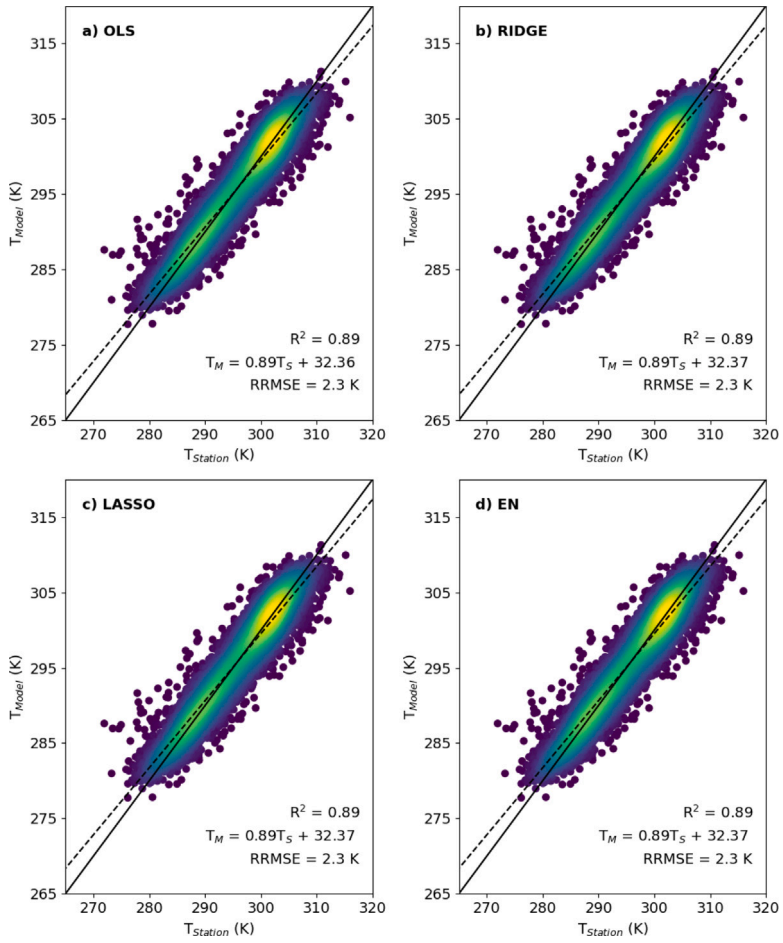

Fig. 9. SAT computed using linear methods for daytime against in situ SAT.

$$SAT = 0.965\ LST - 2.2\ NDVI + 3.1\ AL + 0.195\ U - 0.019\ HR + \\ + 0.027\ Lat - 0.11\ Lon + 0.18\ h + 1.2\ \Delta h + 11.47 \quad (5)$$

LST coefficients are higher than those found by Niclos et al. (2014) (Table 2), demonstrating that, for larger zones, LST has a huge importance on SAT retrieval.

4.3. Nonlinear methods

Results for nonlinear methods show big differences among them. Figs. 11 and 12 show the computed SAT against the station SAT with nonlinear methods. The best method for both daytime and nighttime was XGB, which had the highest correlation, followed by RF model (Figs. 11 and 12). These 2 methods obtained lower RRMSE than linear models for daytime and nighttime (Tables 10 and 11), with a value of 1.8 K at daytime and of 1.2 K at nighttime. XGB outperformed RF, yielding an RRMSE of 1.5 K at daytime and 1.0 K at nighttime. Daytime error was higher than nighttime, but the difference between them was smaller than for previous methods.

KNN and MLP obtained similar results to linear methods: 2.3 K and 2.4 K, respectively, at daytime and 1.3 K and 1.6 K at nighttime. These two methods require a huge amount of data to obtain good results, and thus our dataset is still limited for the accurate performance of KNN and MLP models.

Nonlinear models also let us to know the importance of each variable in our model. Fig. 13 shows the importance of each variable for the best model, i.e. XGB. As for the linear models, LST is the most important variable, specially at nighttime. There is a huge difference between the importance of LST and the other variables. This result implies that an improve of the LST data quality would result in a considerable

Table 8
Daytime linear models' statistics of the differece between in situ SAT and computed SAT.

	OLS (K)	Ridge (K)	Lasso (K)	EN (K)
B	0.03	0.03	0.03	0.03
SD	2.6	2.6	2.6	2.6
RMSE	2.6	2.6	2.6	2.6
Med	0.10	0.10	0.10	0.10
RSD	2.3	2.3	2.3	2.3
RRMSE	2.3	2.3	2.3	2.3

Table 9
Nighttime linear models' statistics of the differece between in situ SAT and computed SAT.

	OLS (K)	Ridge (K)	Lasso (K)	EN (K)
B	−0.06	−0.06	−0.06	−0.06
SD	1.7	1.7	1.7	1.7
RMSE	1.7	1.7	1.7	1.7
Med	−0.06	−0.06	−0.06	−0.05
RSD	1.5	1.5	1.4	1.4
RRMSE	1.5	1.5	1.5	1.5

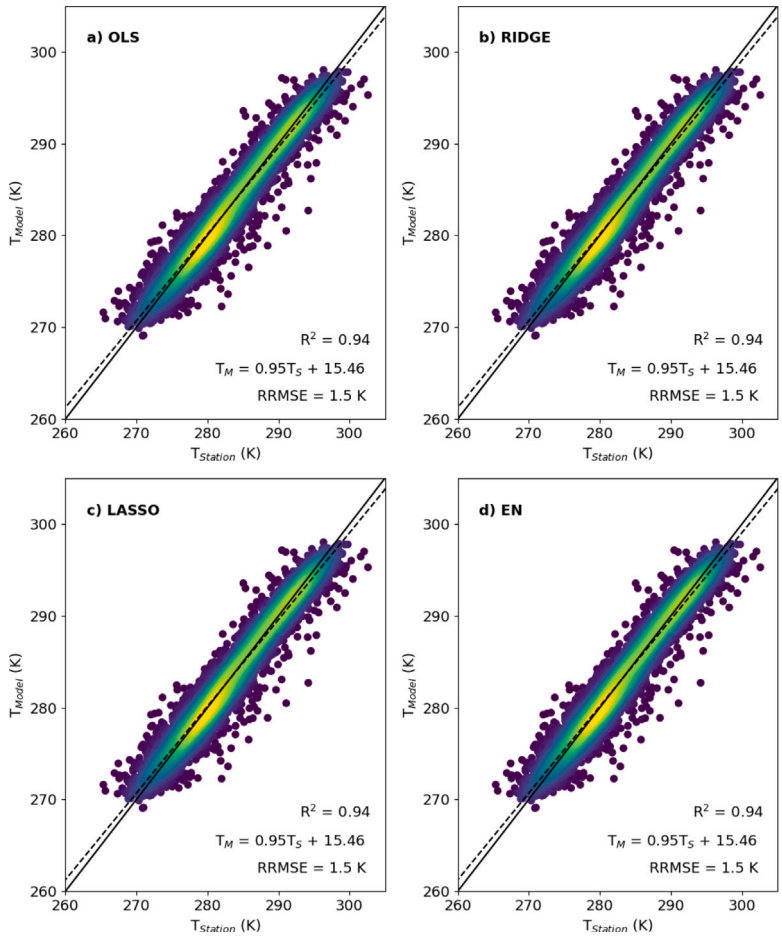

Fig. 10. SAT computed using linear methods for nighttime against in situ SAT.

Table 10
Daytime nonlinear models' statistics of the differece between in situ SAT and computed SAT.

	RF (K)	XGB (K)	KNN (K)	MLP (K)
B	0.02	0.01	0.08	−0.22
SD	2.1	1.7	2.5	2.6
RMSE	2.1	1.7	2.5	2.6
Med	0.03	0.04	0.09	−0.23
RSD	1.8	1.5	2.3	2.4
RRMSE	1.8	1.5	2.3	2.4

Table 11
Nighttime nonlinear models' statistics of the differece between in situ SAT and computed SAT.

	RF (K)	XGB (K)	KNN (K)	MLP (K)
B	−0.05	−0.02	−0.10	0.39
SD	1.5	1.2	1.6	1.8
RMSE	1.5	1.2	1.6	1.8
Med	−0.02	0.06	0.04	0.37
RSD	1.2	1.0	1.3	1.6
RRMSE	1.2	1.0	1.3	1.6

improvement of the model. During daytime, altitude shows also a higher relevance in comparison with the other variables.

In Fig. 14 we compare RRMSEs for the best models of each section. The differences among methods are higher for daytime models, with a difference of 0.8 K between OLS and XGB and between D.6 and OLS. However, the difference between nighttime models is 0.5 K. We also found that daytime models in general obtain worse results than nighttime ones in every method.

XGB algorithm using a moderate amount of data, resulted in the best method to retrieve the SAT, with an uncertainty close to 1.5 K and 1.0 K for daytime and nighttime, respectively.

Although the best results found in this study are comparable to those previously found (Cristóbal et al., 2008; Niclos et al., 2014; Nieto et al., 2011; Noi et al., 2017; Parlak and Yavasoglu, 2023; Prihodko and Goward, 1997; Ruiz-Álvarez et al., 2019; Ye et al., 2022), we used a larger area and period. That makes our models more generalized and, therefore, more flexible when extrapolating to other periods over the same area. Using a larger area and period adds variability (e.g. more seasonal variation, more biomes and larger altitude range) increasing the uncertainty of the models. Thus, we obtained a more robust models which achieve an uncertainty similar or lower than previous studies.

Additionally, we studied the accuracy of the best model, the XGBoost model, in relation to the different landcovers in our study area. We used the CORINE level 1 classification (Büttner and Kosztra, 2011), which shows 4 classes in our study region: artificial surfaces (AS), agricultural areas, (AA), forest and semi-natural areas (FA) and wetlands (W). Table 12 shows similar RRMSE for all of them. The highest value, for both daytime and nighttime model, is obtained for wetlands.

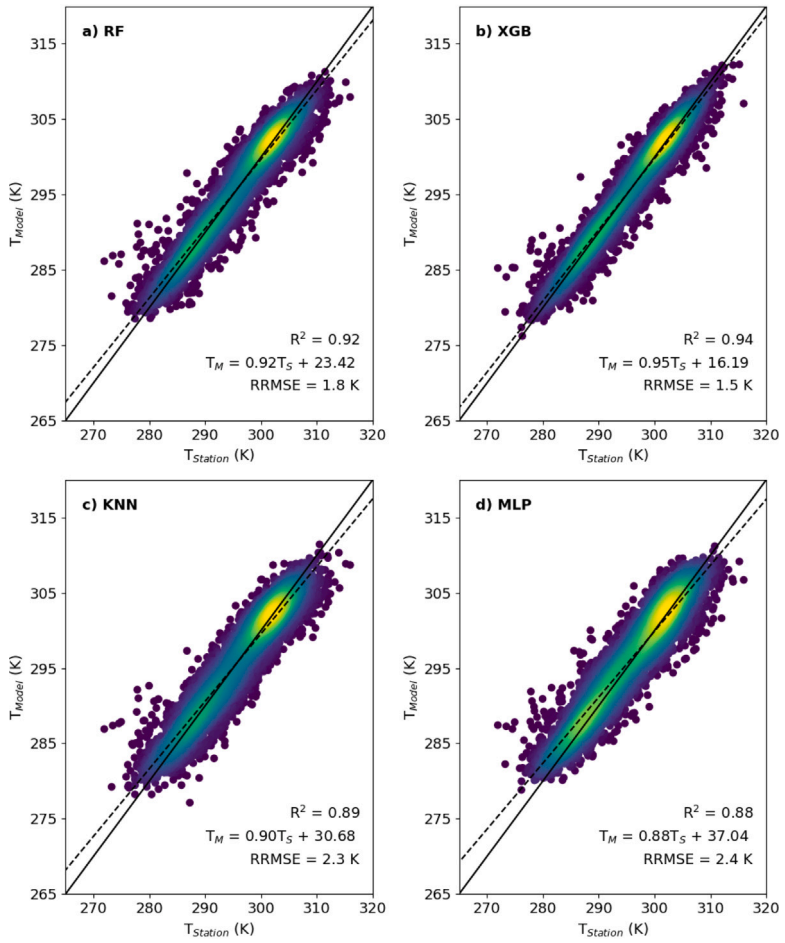

Fig. 11. SAT computed using nonlinear methods for daytime against in situ SAT.

Table 12
Statistics of the daytime and nighttime XGBoost models for the CORINE level 1 landcover classification.

	Daytime				Nighttime			
Statistics	AS	AA	FA	W	AS	AA	FA	W
Med (K)	0.08	0.15	0.20	−0.44	0.06	0.10	0.04	−0.23
RSD (K)	1.5	1.6	1.7	1.8	1.0	1.1	1.2	1.4
RRMSE (K)	**1.5**	**1.6**	**1.7**	**1.9**	**1.0**	**1.1**	**1.2**	**1.4**
Number of data	1683	2398	1129	82	1788	2708	1123	81

However, the percentage of area classified as wetland is negligible compared to the other classes. Thus, according to these results, our daytime and nighttime XGBoost models are well balanced and obtained a similar uncertainty for all landcovers, so these models can be applied for the whole region with a similar performance.

5. Conclusions

Combining remote sensing and reanalysis data makes possible the accurate retrieval of SAT for extense and remote regions without the need of dense networks of ground stations. Spatial and temporal resolutions of input variables are important factors for the precision of the tested models. In this work, reanalysis data had an spatial resolution of 9 km. This resolution is too coarse for the variability of the terrain variables. However, to our knowledge, there is no reanalysis database that offers a better resolution in our study region for the period studied (2021–2022).

Our results agreed with previous publications (Niclos et al., 2014; Ruiz-Álvarez et al., 2019; Tao et al., 2014) and showed that daytime correlations were lower than the nighttime ones. This fact is related to the variability caused by atmospheric heating and solar irradiance. Another factor that affected results was the higher relevance of LST for the nighttime models in comparison with daytime models. However, all the methods had LST as the most important variable. Therefore, an improvement in the accuracy of satellite-derived LST leads to a smaller error in obtaining the SAT for all the methods studied, e.g. with better atmospheric and emissivity corrections.

In this work, we verified that the regressions obtained by Niclos et al. (2014) cannot be extrapolated to study more extensive areas and longer periods. This fact happens because the empirical techniques find the best configuration of coefficients for the input data. Therefore, extrapolation is only possible in datasets with similar characteristics, both spatially and temporally.

Although the existence of linear relationship among input variables used on this work and SAT were demonstrated, the use of nonlinear methods represented an improvement, both for day and night values. While the minimum uncertainties of the linear methods were 2.3 K for daytime and 1.5 K for nighttime, the uncertainties of the nonlinear methods were 1.5 K for daytime and 1.0 K for nighttime. In fact,

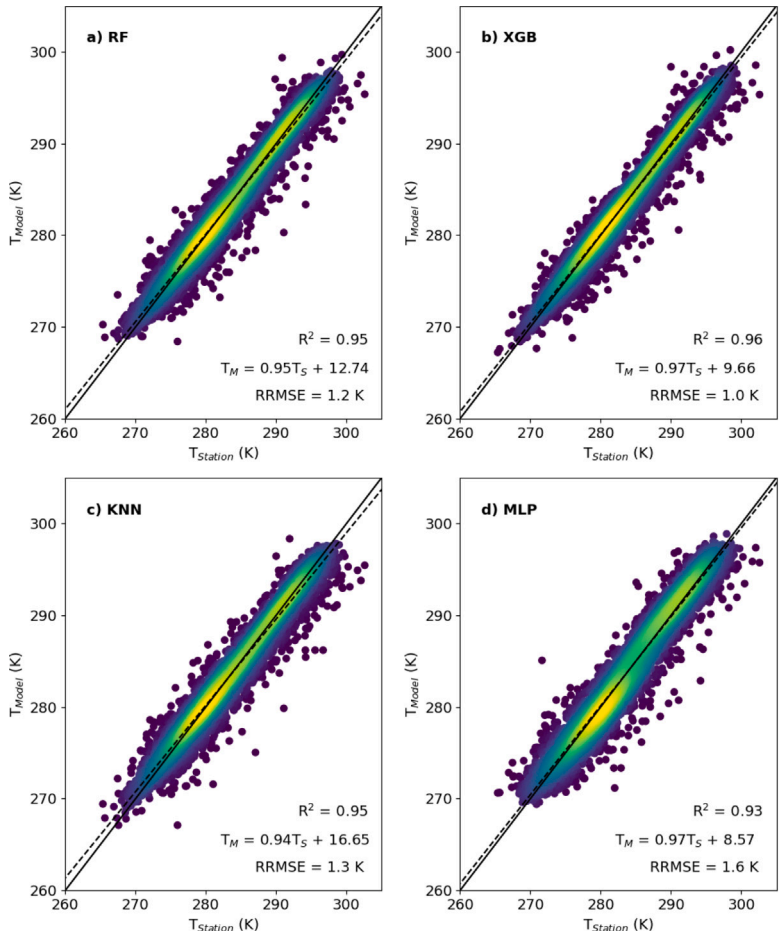

Fig. 12. SAT computed using nonlinear methods for nighttime against in situ SAT.

equation D.6 (the one that works best from Niclos et al., 2014 which was proposed by Zakšek and Schroedter-Homscheidt, 2009) is not a linear equation, since it contains combinations of inputs. D.6 and D.7 equations contain the same variables with different coefficient obtaining completely different results. This fact leads us to affirm that is crucial to characterize your study zone properly, with appropriate variability ranges in variables, because coefficient values have a huge importance in the final result.

Linear methods results showed that, regularized methods do not represent a significant improvement compared to the OLS method in our study. In addition, the simplicity and the lower computational cost of the OLS method are an advantage for its applicability in this case.

Nonlinear methods based on decision trees are the most accurate. Among them, XGB stands out, obtaining a better result than the RF, as it was also observed in Hastie et al. (2009), Shao et al. (2024) and Zhang et al. (2022). However, the MLP neural network and KNN method obtain a similar uncertainty than linear methods and, therefore, the non-parametric methods do not offer any improvement over the linear methods. To sum up, according to our results, the most accurate SAT values were retrieved with XGB method, yielding an RRMSE of 1.5 K at daytime and 1.0 K at nighttime, respectively.

CRediT authorship contribution statement

Joan Vedrí: Writing – original draft, Validation, Software, Methodology, Investigation, Formal analysis, Data curation, Conceptualization. **Raquel Niclòs:** Writing – original draft, Supervision, Methodology, Investigation, Funding acquisition, Conceptualization. **Lluís Pérez-Planells:** Writing – original draft, Supervision, Methodology, Investigation, Conceptualization. **Enric Valor:** Writing – review & editing. **Yolanda Luna:** Resources. **María José Estrela:** Writing – review & editing, Resources, Funding acquisition.

Declaration of competing interest

The authors declare that they have no known competing financial interests or personal relationships that could have appeared to influence the work reported in this paper.

Acknowledgments

The study was conducted within the framework of the project Tool4Extreme PID2020-118797RBI00 funded by Ministerio de Ciencia e Innovacion and Agencia Estatal de Investigacion (MCIN/AEI/10.13039/501100011033). Also, we thanks the project PROMETEO/2021/016 funded by Conselleria de Educacion, Universidades y Empleo, Generalitat Valenciana, Spain.

Data availability

Data will be made available on request.

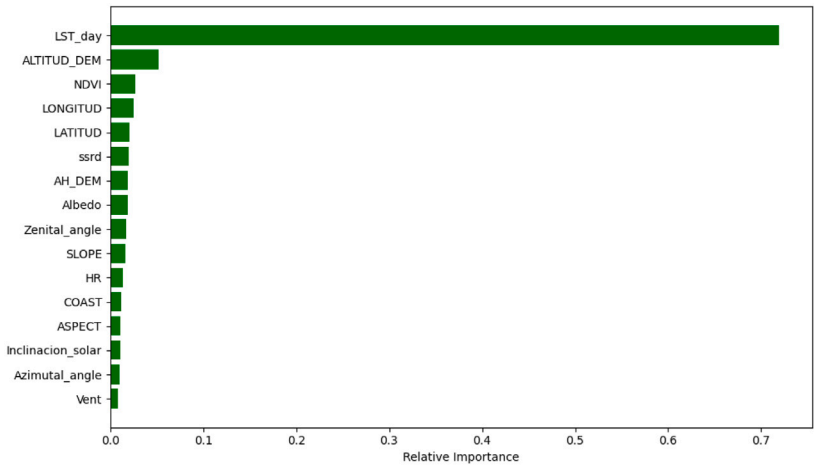

(a) Daytime

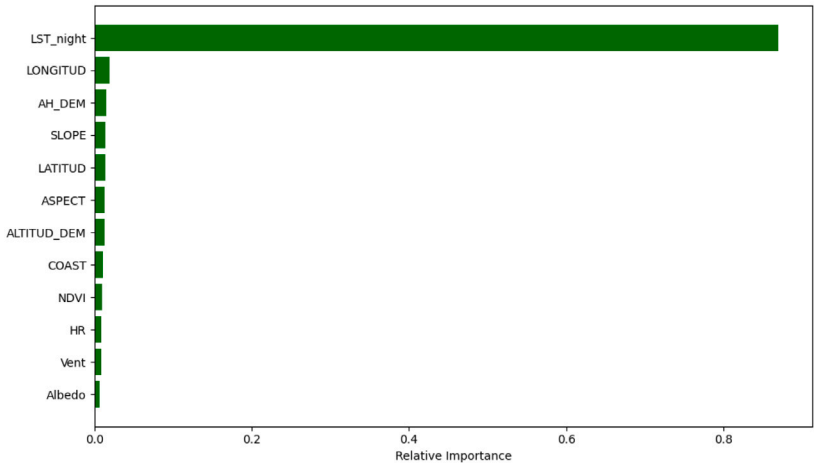

(b) Nighttime

Fig. 13. Feature importance for XGBoost model.

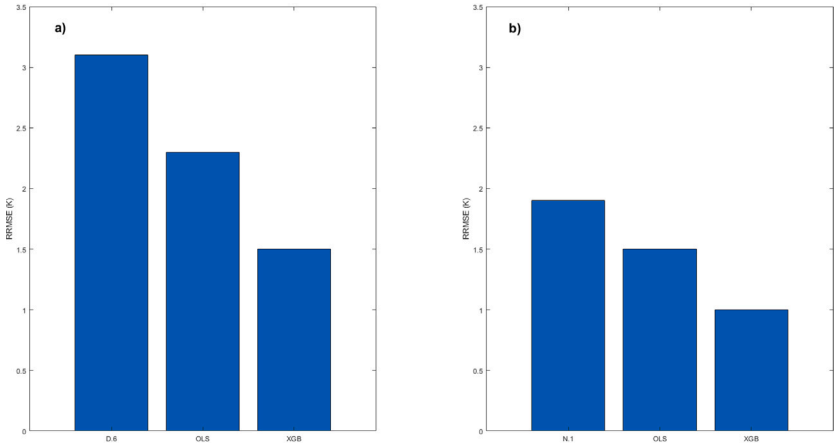

Fig. 14. RRMSE comparison among best models for each method, i.e. eqs. from Niclos et al. (2014), linear methods and nonlinear methods, for (a) daytime and (b) nighttime.

References

Abadi, M., Agarwal, A., Barham, P., Brevdo, E., Chen, Z., et al., 2015. TensorFlow: Large-scale machine learning on heterogeneous systems. https://www.tensorflow.org/. (Accessed 3 July 2024).

AEMET, 2011. Atlas climático ibérico/Iberian climate atlas.

Alduchov, O.A., Eskridge, R.E., 1996. Improved Magnus form approximation of saturation vapor pressure. J. Appl. Meteorol. 35, http://dx.doi.org/10.1175/1520-0450(1996)035<0601:IMFAOS>2.0.CO;2.

August, E.F., 1828. Ueber die Berechnung der Expansivkraft des Wasserdunstes. Ann. Der Phys. 89, http://dx.doi.org/10.1002/andp.18280890511.

Bian, Z., Roujean, J.L., Fan, T., Dong, Y., Hu, T., Cao, B., Li, H., Du, Y., Xiao, Q., Liu, Q., 2023. An angular normalization method for temperature vegetation dryness index (TVDI) in monitoring agricultural drought. Remote Sens. Environ. 284, http://dx.doi.org/10.1016/j.rse.2022.113330.

Bladé, I., Castro-Díez, Y., 2010. Tendencias atmosféricas en la Península Ibérica durante el periodo instrumental en el contexto de la variabilidad natural. Clima de España: Pasado Presente y Futuro. Informe de Evaluación del Cambio Climático Regional. Red Climática. CLIVAR-ESPAÑA, Madrid,

Brugnara, Y., Good, E., Squintu, A.A., van der Schrier, G., Brönnimann, S., 2019. The EUSTACE global land station daily air temperature dataset. Geosci. Data J. 6, http://dx.doi.org/10.1002/gdj3.81.

Büttner, G., Kosztra, B., 2011. Manual of CORINE land cover changes. Eur. Env. Agency.

Chen, T., Guestrin, C., 2016. XGBoost: A scalable tree boosting system. In: Proceedings of the ACM SIGKDD International Conference on Knowledge Discovery and Data Mining 13-17-August-2016. http://dx.doi.org/10.1145/2939672.2939785.

Cover, T.M., Hart, P.E., 1967. Nearest neighbor pattern classification. IEEE Trans. Inform. Theory 13, http://dx.doi.org/10.1109/TIT.1967.1053964.

Cristóbal, J., Ninyerola, M., Pons, X., 2008. Modeling air temperature through a combination of remote sensing and GIS data. J. Geophys. Res.: Atmos. 113, http://dx.doi.org/10.1029/2007JD009318.

Czajkowski, K.P., Goward, S.N., Stadler, S.J., Walz, A., 2000. Thermal remote sensing of near surface environmental variables: Application over the Oklahoma Mesonet. Prof. Geogr. 52, 345–357. http://dx.doi.org/10.1111/0033-0124.00230.

Diffenbaugh, N.S., Giorgi, F., 2012. Climate change hotspots in the CMIP5 global climate model ensemble. Clim. Change 114, http://dx.doi.org/10.1007/s10584-012-0570-x.

Dunn, R., 2020. Met Office Hadley Centre observations datasets. https://www.metoffice.gov.uk/hadobs/hadex3/. (Accessed 04 September 2024).

Dunn, R.J., Alexander, L.V., Donat, M.G., Zhang, X., Bador, M., et al., 2020. Development of an updated global land in situ-based data set of temperature and precipitation extremes: HadEX3. J. Geophys. Res.: Atmos. 125, http://dx.doi.org/10.1029/2019JD032263.

EEA, 2017. EEA coastline for analysis. https://www.eea.europa.eu/data-and-maps/data/eea-coastline-for-analysis-2. (Accessed 5 May 2024).

Fix, E., Hodges, J.L., 1989. Discriminatory analysis. Nonparametric discrimination: Consistency properties. Int. Stat. Rev. / Rev. Int. de Stat. 57, http://dx.doi.org/10.2307/1403797.

Font Tullot, I., 2000. Climatología de españa y Portugal.

GCOS, 2022. The 2022 GCOS Implementation Plan (GCOS-244). World Meteorological Organization (WMO).

Ghent, D., Veal, K., Trent, T., Dodd, E., Sembhi, H., Remedios, J., 2019. A new approach to defining uncertainties for MODIS land surface temperature. Remote Sens. 11, http://dx.doi.org/10.3390/rs11091021.

Gomis-Cebolla, J., Rattayova, V., Salazar-Galán, S., Francés, F., 2023. Evaluation of ERA5 and ERA5-land reanalysis precipitation datasets over Spain (1951–2020). Atmos. Res. 284, http://dx.doi.org/10.1016/j.atmosres.2023.106606.

Gonzalez-Hidalgo, J.C., Peña-Angulo, D., Brunetti, M., Cortesi, N., 2015. MOTEDAS: A new monthly temperature database for mainland Spain and the trend in temperature (1951–2010). Int. J. Climatol. 35, http://dx.doi.org/10.1002/joc.4298.

Good, E., 2015. Daily minimum and maximum surface air temperatures from geostationary satellite data. J. Geophys. Res. 120, http://dx.doi.org/10.1002/2014JD022438.

Good, E., 2016. An in situ-based analysis of the relationship between land surface skin and screen-level air temperatures. J. Geophys. Res. 121, http://dx.doi.org/10.1002/2016JD025318.

Good, E., Ghent, D.J., Bulgin, C.E., Remedios, J.J., 2017. A spatiotemporal analysis of the relationship between near-surface air temperature and satellite land surface temperatures using 17 years of data from the ATSR series. J. Geophys. Res.: Atmos. 122, http://dx.doi.org/10.1002/2017JD026880.

Hastie, T., Tibshirani, R., Friedman, J., 2009. Springer series in statistics: The elements of statistical learning: Data mining, inference and prediction.

Hayashi, F., 2000. Econometrics. http://dx.doi.org/10.4337/9781788975971.00009.

Hoerl, A.E., Kennard, R.W., 1970. Ridge regression: Biased estimation for nonorthogonal problems. Technometrics 12, http://dx.doi.org/10.1080/00401706.1970.10488634.

Huete, A., Justice, C., 1999. MODIS vegetation index (MOD 13) algorithm theoretical basis document. Remote Sens. Environ. 3.

IGN, 2010. Instituto Geográfico Nacional. https://www.ign.es/web/ign/portal/qsm-cnig. (Accessed 4 June 2024).

James, G., Witten, D., Hastie, T., Tibshirani, R., 2013. An Introduction to Statistical Learning with Applications in R.

Jeng, Y.J., Martin, A., 1985. Residuals in multiple regression analysis. J. Pharm. Sci. 74, http://dx.doi.org/10.1002/jps.2600741006.

Khesali, E., Mobasheri, M., 2020. A method in near-surface estimation of air temperature (NEAT) in times following the satellite passing time using MODIS images. Adv. Space Res. 65, http://dx.doi.org/10.1016/j.asr.2020.02.006.

Khesali, E., Mobasheri, M.R., 2023. Near surface air temperature estimation through parametrization of modis products. ISPRS Ann. Photogramm. Remote. Sens. Spat. Inf. Sci. 10, http://dx.doi.org/10.5194/isprs-annals-X-4-W1-2022-405-2023.

Lawrence, M.G., 2005. The relationship between relative humidity and the dewpoint temperature in moist air: A simple conversion and applications. Bull. Am. Meteorol. Soc. 86, http://dx.doi.org/10.1175/BAMS-86-2-225.

León-Tavares, J., Roujean, J.L., Smets, B., Wolters, E., Toté, C., Swinnen, E., 2021. Correction of directional effects in vegetation ndvi time-series. Remote Sens. 13, http://dx.doi.org/10.3390/rs13061130.

Lionello, P., Scarascia, L., 2018. The relation between climate change in the Mediterranean region and global warming. Reg. Environ. Chang. 18, http://dx.doi.org/10.1007/s10113-018-1290-1.

Lorenzo, M.N., Alvarez, I., 2022. Future changes of hot extremes in Spain: towards warmer conditions. Nat. Hazards 113, http://dx.doi.org/10.1007/s11069-022-05306-x.

Lorenzo, N., Díaz-Poso, A., Royé, D., 2021. Heatwave intensity on the Iberian Peninsula: Future climate projections. Atmos. Res. 258, http://dx.doi.org/10.1016/j.atmosres.2021.105655.

Magnus, G., 1844. Versuche über die Spannkräfte des Wasserdampfs. Ann. Der Phys. 137, http://dx.doi.org/10.1002/andp.18441370202.

MedECC, 2020. Climate and environmental change in the mediterranean basin - current situation and risks for the future, first mediterranean assessmnet report.

Miró, J.J., Estrela, M.J., Caselles, V., Gómez, I., 2018. Spatial and temporal rainfall changes in the Júcar and Segura basins (1955–2016): Fine-scale trends. Int. J. Climatol. 38, http://dx.doi.org/10.1002/joc.5689.

Montavon, G., Orr, G.B., Müller, K.-R., 2012. Neural networks: Tricks of the trade.

Muñoz-Sabater, J., Dutra, E., Agustí-Panareda, A., Albergel, C., Arduini, G., et al., 2021. ERA5-land: A state-of-the-art global reanalysis dataset for land applications. Earth Syst. Sci. Data 13, http://dx.doi.org/10.5194/essd-13-4349-2021.

Niclos, R., Valiente, J.A., Barbera, M.J., Caselles, V., 2014. Land surface air temperature retrieval from eos-modis images. IEEE Geosci. Remote. Sens. Lett. 11, http://dx.doi.org/10.1109/LGRS.2013.2293540.

Nieto, H., Sandholt, I., Aguado, I., Chuvieco, E., Stisen, S., 2011. Air temperature estimation with MSG-SEVIRI data: Calibration and validation of the TVX algorithm for the Iberian Peninsula. Remote Sens. Environ. 115, http://dx.doi.org/10.1016/j.rse.2010.08.010.

Ninyerola, M., Pons, X., Roure, J.M., 2007. Objective air temperature mapping for the Iberian Peninsula using spatial interpolation and GIS. Int. J. Climatol. 27, http://dx.doi.org/10.1002/joc.1462.

Noi, P.T., Degener, J., Kappas, M., 2017. Comparison of multiple linear regression, cubist regression, and random forest algorithms to estimate daily air surface temperature from dynamic combinations of MODIS LST data. Remote Sens. 9, http://dx.doi.org/10.3390/rs9050398.

Olcina, J., Serrano-Notivoli, R., Miró, J., Meseguer-Ruiz, O., 2019. Tropical nights on the Spanish Mediterranean coast, 1950–2014. Clim. Res. 78, http://dx.doi.org/10.3354/cr01569.

Paredes-Fortuny, L., Khodayar, S., 2023. Understanding the Magnification of Heatwaves over Spain: Relevant changes in the most extreme events. Weather. Clim. Extrem. 42, http://dx.doi.org/10.1016/j.wace.2023.100631.

Parlak, B.O., Yavasoglu, H.A., 2023. Comparison of regression algorithms to predict average air temperature. Uluslararas Muhendis. Arastirma Ve Gelistirme Derg. 15, http://dx.doi.org/10.29137/umagd.1232020.

Pedregosa, F., Varoquaux, G., Gramfort, A., Michel, V., Thirion, B., et al., 2011a. Scikit-learn: Machine learning in Python. J. Mach. Learn. Res. 12.

Pedregosa, F., Varoquaux, G., Gramfort, A., Michel, V., Thirion, B., et al., 2011b. User guide: contents — scikit-learn 0.23.2 documentation. JMLR 12.

Pérez-Planells, L., Niclòs, R., Puchades, J., Coll, C., Göttsche, F.M., Valiente, J.A., Valor, E., Galve, J.M., 2021. Validation of sentinel-3 slstr land surface temperature retrieved by the operational product and comparison with explicitly emissivity-dependent algorithms. Remote Sens. 13, http://dx.doi.org/10.3390/rs13112228.

Pompeu, C.R., Peñas, F.J., Belmar, O., Barquín, J., 2023. Large-scale factors controlling biological communities in the Iberian Peninsula: an insight into global change effects on river ecosystems. Aquat. Sci. 85, http://dx.doi.org/10.1007/s00027-023-00995-3.

Prihodko, L., Goward, S.N., 1997. Estimation of air temperature from remotely sensed surface observations. Remote Sens. Environ. 60, http://dx.doi.org/10.1016/S0034-4257(96)00216-7.

Recondo, C., Peón, J.J., Zapico, E., Pendás, E., 2013. Empirical models for estimating daily surface water vapour pressure, air temperature, and humidity using MODIS and spatiotemporal variables. Applications to Peninsular Spain. Int. J. Remote Sens. 34, http://dx.doi.org/10.1080/01431161.2013.828185.

Ruiz-Álvarez, M., Alonso-Sarria, F., Gomariz-Castillo, F., 2019. Interpolation of instantaneous air temperature using geographical and MODIS derived variables with machine learning techniques. ISPRS Int. J. Geo-Inf. 8, http://dx.doi.org/10.3390/ijgi8090382.

Schelldorfer, J., Bühlmann, P., Geer, S.V.D., 2011. Estimation for high-dimensional linear mixed-effects models using l1-penalization. Scandinavian J. Stat. 38, http://dx.doi.org/10.1111/j.1467-9469.2011.00740.x.

Shao, Z., Ahmad, M.N., Javed, A., 2024. Comparison of random forest and XGBoost classifiers using integrated optical and SAR features for mapping urban impervious surface. Remote Sens. 16, http://dx.doi.org/10.3390/rs16040665.

Stocker, T., Qin, D., Plattner, G., Tignor, M., Allen, S., Boschung, J., Xia, A.N.Y., Bex, V., Midgley, P., 2023. Climate Change 2021 – The Physical Science Basis. http://dx.doi.org/10.1017/9781009157896.

Strahler, A.H., Muller, J.P., 1999. MODIS BRDF albedo product : Algorithm theoretical basis document. MODIS Product ID: MOD43 Version 5.

Tao, J., Zhang, Y., Zhu, J., Jiang, Y., Zhang, X., Zhang, T., Xi, Y., 2014. Elevation-dependent temperature change in the Qinghai–Xizang Plateau grassland during the past decade. Theor. Appl. Climatol. 117, http://dx.doi.org/10.1007/s00704-013-0976-z.

Tibshirani, R., 1996. Regression shrinkage and selection via the Lasso. J. R. Stat. Soc. Ser. B: Methodol. 58, http://dx.doi.org/10.1111/j.2517-6161.1996.tb02080.x.

Tibshirani, R., 2011. Regression shrinkage and selection via the lasso: A retrospective. J. R. Stat. Soc. Ser. B Stat. Methodol. 73, http://dx.doi.org/10.1111/j.1467-9868.2011.00771.x.

Valor, E., Puchades, J., Niclos, R., Romero, J.M.G., Lacave, O., Puig, P., 2023. Determination and evaluation of surface solar irradiance with the MAGIC-Heliosat method adapted to MTSAT-2/Imager and Himawari-8/AHI sensors. IEEE Trans. Geosci. Remote Sens. 61, http://dx.doi.org/10.1109/TGRS.2023.3238180.

Wan, Z., 1999. MODIS Land-Surface Temperature Algorithm Theoretical Basis Document (LST ATBD). Institute for Computational Earth System Science, Santa Barbara.

Williams, M.N., Grajales, C.A.G., Kurkiewicz, D., 2013. Assumptions of multiple regression: Correcting two misconceptions. Pr. Assess. Res. Eval. 18.

Wilrich, P.T., 2007. Robust estimates of the theoretical standard deviation to be used in interlaboratory precision experiments. Accrédit. Qual. Assur. 12, http://dx.doi.org/10.1007/s00769-006-0240-7.

Ye, X., Mei, X., Zhong, S., Wang, M., Song, D., 2022. Air temperature estimates using deep learning regression. In: 2022 10th International Conference on Agro-Geoinformatics, Agro-Geoinformatics 2022. http://dx.doi.org/10.1109/Agro-Geoinformatics55649.2022.9859152.

Zakšek, K., Schroedter-Homscheidt, M., 2009. Parameterization of air temperature in high temporal and spatial resolution from a combination of the SEVIRI and MODIS instruments. ISPRS J. Photogramm. Remote Sens. 64, http://dx.doi.org/10.1016/j.isprsjprs.2009.02.006.

Zhang, Y., Liu, J., Shen, W., 2022. A review of ensemble learning algorithms used in remote sensing applications. Appl. Sci. (Switzerland) 12, http://dx.doi.org/10.3390/app12178654.

Zou, H., Hastie, T., 2005. Regularization and variable selection via the elastic net. J. R. Stat. Soc. Ser. B Stat. Methodol. 67, http://dx.doi.org/10.1111/j.1467-9868.2005.00503.x.